

EXACT SPIKE TRAIN INFERENCE VIA ℓ_0 OPTIMIZATION

BY SEAN JEWELL¹ AND DANIELA WITTEN²

University of Washington

In recent years new technologies in neuroscience have made it possible to measure the activities of large numbers of neurons simultaneously in behaving animals. For each neuron a *fluorescence trace* is measured; this can be seen as a first-order approximation of the neuron’s activity over time. Determining the exact time at which a neuron spikes on the basis of its fluorescence trace is an important open problem in the field of computational neuroscience.

Recently, a convex optimization problem involving an ℓ_1 penalty was proposed for this task. In this paper we slightly modify that recent proposal by replacing the ℓ_1 penalty with an ℓ_0 penalty. In stark contrast to the conventional wisdom that ℓ_0 optimization problems are computationally intractable, we show that the resulting optimization problem can be efficiently solved for the global optimum using an extremely simple and efficient dynamic programming algorithm. Our R-language implementation of the proposed algorithm runs in a few minutes on fluorescence traces of 100,000 timesteps. Furthermore, our proposal leads to substantial improvements over the previous ℓ_1 proposal, in simulations as well as on two calcium imaging datasets.

R-language software for our proposal is available on CRAN in the package `LZeroSpikeInference`. Instructions for running this software in python can be found at <https://github.com/jewellsean/LZeroSpikeInference>.

1. Introduction. When a neuron spikes, calcium floods the cell. In order to quantify intracellular calcium levels, calcium imaging techniques make use of fluorescent calcium indicator molecules [Ahrens et al. (2013), Dombbeck et al. (2007), Prevedel et al. (2014)]. Thus, a neuron’s *fluorescence trace* can be seen as a first-order approximation of its activity level over time.

However, the fluorescence trace itself is typically not of primary scientific interest; instead, it is of interest to determine the underlying neural activity, that is, the specific times at which the neuron spiked. Inferring the spike times on the basis of a fluorescence trace amounts to a challenging deconvolution problem, which has been the focus of substantial investigation [Deneux et al. (2016), Grewe et al. (2010), Pnevmatikakis et al. (2013), Sasaki et al. (2008), Theis et al. (2016), Vogelstein et al. (2009, 2010), Holekamp, Turaga and Holy (2008), Yaksi and Friedrich (2006), Friedrich and Paninski (2016), Friedrich, Zhou and Paninski

Received November 2017.

¹Supported by the Natural Sciences and Engineering Research Council of Canada.

²Supported in part by NIH Grant DP5OD009145 and NSF CAREER Award DMS-1252624.

Key words and phrases. Neuroscience, calcium imaging, changepoint detection, dynamic programming.

(2017)]. In this paper we propose a new approach for this task, which is based upon the following insight, an autoregressive model for calcium dynamics that has been extensively studied in the neuroscience literature [Friedrich and Paninski (2016), Friedrich, Zhou and Paninski (2017), Vogelstein et al. (2010)] leads directly to a simple ℓ_0 optimization problem for which an efficient and exact algorithm is available.

1.1. *An autoregressive model for calcium dynamics.* In this paper we will revisit an autoregressive model for calcium dynamics that has been considered by a number of authors in the recent literature [Friedrich and Paninski (2016), Friedrich, Zhou and Paninski (2017), Pnevmatikakis et al. (2016), Vogelstein et al. (2010)]. We closely follow the notation of Friedrich, Zhou and Paninski (2017). This model posits that y_t , the fluorescence at the t th timestep, is a noisy realization of c_t , the unobserved underlying calcium concentration at the t th timestep. In the absence of a spike at the t th timestep ($s_t = 0$), the calcium concentration decays according to a p th-order autoregressive process. However, if a spike occurs at the t th timestep ($s_t > 0$), then the calcium concentration increases. Thus,

$$\begin{aligned}
 & y_t = \beta_0 + \beta_1 c_t + \varepsilon_t, \quad \varepsilon_t \sim_{\text{ind.}} (0, \sigma^2), \quad t = 1, \dots, T; \\
 (1) \quad & c_t = \sum_{i=1}^p \gamma_i c_{t-i} + s_t, \quad t = p + 1, \dots, T.
 \end{aligned}$$

In (1), the quantities $\gamma_1, \dots, \gamma_p$ are the parameters in the autoregressive model. Note that the quantity y_t in (1) is observed; all other quantities are unobserved. Since we would like to know whether a spike occurred at the t th timestep, the parameter of interest is s_t . Figure 1(a) displays a small dataset generated according to (1).

In what follows, for ease of exposition, we assume $\beta_0 = 0$ and $\beta_1 = 1$ in (1). This assumption is made without loss of generality, since β_0 and β_1 can be estimated from the data, and the observed fluorescence y_1, \dots, y_T centered and scaled accordingly. See Section 5 for additional details.

Vogelstein et al. (2010), Friedrich and Paninski (2016) and Friedrich, Zhou and Paninski (2017) seek to interpret s_t in (1) as the *number* of spikes at the t th timestep. Thus, in principle it would be desirable to use a count-valued distribution, such as the Poisson distribution, as a prior on s_t . However, because maximum a posteriori estimation of s_t in (1) using a Poisson distribution is computationally intractable, they instead suppose that s_t has an exponential distribution [Vogelstein et al. (2010)]. In the case of the first-order autoregressive process ($p = 1$), this leads Vogelstein et al. (2010) to the optimization problem

$$\begin{aligned}
 (2) \quad & \underset{c_1, \dots, c_T, s_2, \dots, s_T}{\text{minimize}} \left\{ \frac{1}{2} \sum_{t=1}^T (y_t - c_t)^2 + \lambda \sum_{t=2}^T |s_t| \right\} \\
 & \text{subject to } s_t = c_t - \gamma c_{t-1} \geq 0,
 \end{aligned}$$

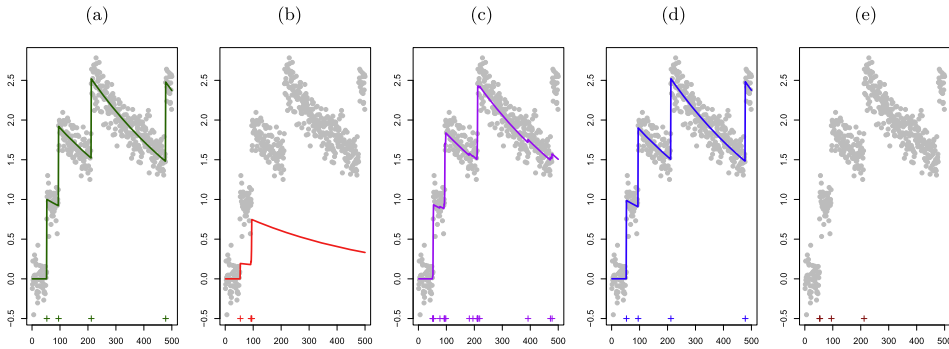


FIG. 1. A toy simulated data example. In each panel the x -axis represents time. Observed fluorescence values are displayed in (\bullet) . (a): Unobserved calcium concentrations (—) and true spike times $(+)$. Data were generated according to the model (1). (b): Estimated calcium concentrations (—) and spike times $(+)$ that result from solving the ℓ_1 optimization problem (3) with the value of λ that yields the true number of spikes. This value of λ leads to very poor estimation of both the underlying calcium dynamics and the spikes. (c): Estimated calcium concentrations (—) and spike times $(+)$ that result from solving the ℓ_1 optimization problem (3) with the largest value of λ that results in at least one estimated spike within the vicinity of each true spike. This value of λ results in 19 estimated spikes, which is far more than the true number of spikes. The poor performance of the ℓ_1 optimization problem in panels (b) and (c) is a consequence of the fact that the ℓ_1 penalty performs shrinkage as well as spike estimation; this is discussed further in Section 1.2. (d): Estimated calcium concentrations (—) and spike times $(+)$ that result from solving the ℓ_0 optimization problem (5). (e): The four spikes in panel (c) associated with the largest estimated increase in calcium $(+)$; we refer to this in the text as the post-thresholding ℓ_1 estimator. Since the estimated calcium is not well defined after post-thresholding, we do not plot the estimated calcium concentration.

where λ is a nonnegative tuning parameter that controls the tradeoff between the fit of the estimated calcium to the observed fluorescence and the sparsity of the estimated spike vector $\hat{s}_2, \dots, \hat{s}_T$. Friedrich and Paninski (2016) and Friedrich, Zhou and Paninski (2017) instead consider a closely related problem that results from including an additional ℓ_1 penalty for the initial calcium concentration,

$$(3) \quad \underset{c_1, \dots, c_T, s_2, \dots, s_T}{\text{minimize}} \left\{ \frac{1}{2} \sum_{t=1}^T (y_t - c_t)^2 + \lambda |c_1| + \lambda \sum_{t=2}^T |s_t| \right\}$$

subject to $s_t = c_t - \gamma c_{t-1} \geq 0$.

Both (2) and (3) are convex optimization problems, which can be solved for the global optimum using a well-developed set of optimization algorithms [Bien and Witten (2016), Boyd and Vandenberghe (2004), Hastie, Tibshirani and Friedman (2009), Hastie, Tibshirani and Wainwright (2015)]. Because $\hat{s}_2, \dots, \hat{s}_T$ are not integer valued, they cannot be directly interpreted as the number of spikes at each timestep; however, informally, a larger value of \hat{s}_t can be interpreted as indicating greater certainty that one or more spikes occurred at the t th timestep.

In this paper we reconsider the model (1) that originally motivated the optimization problems (2) and (3) in the recent literature [Friedrich and Paninski (2016), Friedrich, Zhou and Paninski (2017), Vogelstein et al. (2010)]. Rather than interpreting s_t in (1) as the number of spikes at the t th timestep, we interpret its sign as an indicator for whether or not at least one spike occurred, that is, $s_t = 0$ indicates no spikes at the t th timestep, and $s_t > 0$ indicates the occurrence of at least one spike. Then, in the case of a first-order autoregressive model ($p = 1$), (1) leads naturally to the optimization problem

$$(4) \quad \begin{aligned} & \underset{c_1, \dots, c_T, s_2, \dots, s_T}{\text{minimize}} \left\{ \frac{1}{2} \sum_{t=1}^T (y_t - c_t)^2 + \lambda \sum_{t=2}^T 1_{(s_t \neq 0)} \right\} \\ & \text{subject to } s_t = c_t - \gamma c_{t-1} \geq 0, \end{aligned}$$

where $1_{(A)}$ is an indicator variable that equals 1 if the event A holds and 0 otherwise. In (4) λ is a nonnegative tuning parameter that controls the tradeoff between the fit of the estimated calcium to the observed fluorescence and the number of timesteps at which a spike is estimated to occur.

Unfortunately, the optimization problem (4) is highly nonconvex due to the presence of the indicator variable. In the statistics literature this term is known as an ℓ_0 penalty. It is well known that optimization involving ℓ_0 penalties is typically computationally intractable; in general no efficient algorithms are available to solve for the global optimum.

In fact the convex optimization problem (2) considered in Vogelstein et al. (2010) and its close cousin (3) considered in Friedrich and Paninski (2016) and Friedrich, Zhou and Paninski (2017), can be viewed as convex relaxations to the problem (4). That is, if we replace the ℓ_0 penalty in (4) with an ℓ_1 penalty, then we arrive exactly at problem (2).

1.2. Contribution of this paper. In the previous subsection we established that the optimization problems (2) and (3) studied by Vogelstein et al. (2010), Friedrich and Paninski (2016) and Friedrich, Zhou and Paninski (2017) can be seen as convex relaxations of the ℓ_0 optimization problem (4), which follows directly from the model (1). In fact under the model (1), (4) is the “right” optimization problem to be solving; (2) and (3) are simply computationally tractable approximations to this problem. In fact, Friedrich, Zhou and Paninski (2017) allude to this in the “Hard shrinkage and ℓ_0 penalty” section of their paper.

However, using an ℓ_1 norm to approximate an ℓ_0 norm comes with computational advantages at the expense of substantial performance disadvantages; in particular, the use of an ℓ_1 penalty tends to *overshrink* the fitted estimates [Zou (2006)]. This can be seen quite clearly in Figures 1(b) and 1(c). Retaining only the four spikes in Figure 1(c) associated with the largest increases in calcium leads

to an improvement in spike detection [Figure 1(e); this is referred to as the *post-thresholding ℓ_1 estimator* in what follows], but still one of the four true spikes is missed.

In this paper we consider a slight modification of (4) that results from removing the positivity constraint,

$$(5) \quad \begin{aligned} & \underset{c_1, \dots, c_T, s_2, \dots, s_T}{\text{minimize}} \left\{ \frac{1}{2} \sum_{t=1}^T (y_t - c_t)^2 + \lambda \sum_{t=2}^T 1_{(s_t \neq 0)} \right\} \\ & \text{subject to } s_t = c_t - \gamma c_{t-1}. \end{aligned}$$

In practice the distinction between the problems (5) and (4) is quite minor; on real data applications, for appropriate choices of the decay rate γ , the solution to (5) tends to satisfy the constraint in (4), and so the solutions are identical.

Like problem (4), solving problem (5) for the global optimum appears, at a glance, to be computationally intractable—we (the authors) are only aware of a few ℓ_0 optimization problems for which exact solutions can be obtained via efficient algorithms.

However, in this paper we show that in fact (5) is a rare ℓ_0 optimization problem that can be *exactly solved for the global optimum using an efficient algorithm*. This is because (5) can be seen as a changepoint detection problem for which efficient algorithms that run in no more than $\mathcal{O}(T^2)$ time, and often closer to $\mathcal{O}(T)$ time, are available. Furthermore, our implementation of the exact algorithm for solving (5) yields excellent results relative to the convex approximation (3) considered by Friedrich and Paninski (2016) and Friedrich, Zhou and Paninski (2017). This vastly improved performance can be seen in Figure 1(d).

The rest of this paper is organized as follows. In Section 2 we present an exact algorithm for solving the ℓ_0 problem (5). In Section 3 we investigate the performance of this algorithm, relative to the algorithm of Friedrich and Paninski (2016) and Friedrich, Zhou and Paninski (2017) for solving the ℓ_1 problem (3) in a simulation study. In Section 4 we investigate the performances of both algorithms for spike train inference on a dataset for which the true spike times are known [Chen et al. (2013), GENIE Project (2015)] and on a dataset from the Allen Brain Observatory [Allen Institute for Brain Science (2016), Hawrylycz et al. (2016)]. In Section 5 we generalize the problem (5) in order to allow for efficient estimation of an intercept term and to accommodate an autoregressive model of order $p > 1$ (1). Finally, we close with a discussion in Section 6. Technical details and additional results can be found in the Appendix.

2. An exact algorithm for solving problem (5). In Section 2.1 we show that problem (5) can be viewed as a changepoint detection problem. In Sections 2.2 and 2.3 we apply existing algorithms for changepoint detection in order to efficiently solve (5) for the global optimum in $\mathcal{O}(T^2)$ and in substantially fewer than

$O(T^2)$ operations, respectively. Timing results are presented in Section 2.4. We discuss selection of the tuning parameter λ and autoregressive parameter γ in (5) in Appendix B.

2.1. *Recasting (5) as a changepoint detection problem.* Recall that our goal is to solve the ℓ_0 optimization problem (5) or, equivalently, to compute $\hat{c}_1, \dots, \hat{c}_T$ that solve the optimization problem

$$\text{minimize}_{c_1, \dots, c_T} \left\{ \frac{1}{2} \sum_{t=1}^T (y_t - c_t)^2 + \lambda \sum_{t=2}^T 1_{(c_t - \gamma c_{t-1} \neq 0)} \right\}.$$

We estimate a spike event at the t th timestep if $\hat{c}_t \neq \gamma \hat{c}_{t-1}$. (We refer to this as a “spike event,” rather than a spike, since $\hat{c}_t \neq \gamma \hat{c}_{t-1}$ indicates the presence of at least one spike at the t th timepoint, but does not directly provide an estimate of the number of spikes.) We now make two observations about this optimization problem:

1. Given that a spike event is estimated at the t th timestep, the estimated calcium concentration at any time $t_1 < t$ is independent of the estimated calcium concentration at any time $t_2 \geq t$.
2. Given that two spike events are estimated at the t th and t' th timesteps with $t < t'$, and no spike events are estimated in between the t th and t' th timesteps, the calcium concentration is estimated to decay exponentially between the t th and t' th timesteps.

This motivates us to consider the relationship between (5) and a *changepoint detection problem* [Aue and Horváth (2013), Braun and Müller (1998), Davis, Lee and Rodriguez-Yam (2006), Yao (1988), Lee (1995), Jackson et al. (2005), Killick, Fearnhead and Eckley (2012), Maidstone et al. (2017)] of the form

$$(6) \quad \text{minimize}_{0=\tau_0 < \tau_1 < \dots < \tau_k < \tau_{k+1}=T, k} \left\{ \sum_{j=0}^k \mathcal{D}(y_{(\tau_j+1):\tau_{j+1}}) + \lambda k \right\},$$

where

$$(7) \quad \mathcal{D}(y_{a:b}) \equiv \min_{c_a, c_t = \gamma c_{t-1}, t=a+1, \dots, b} \left\{ \frac{1}{2} \sum_{t=a}^b (y_t - c_t)^2 \right\}.$$

In (6) we are simultaneously minimizing the objective over the times at which the changepoints (τ_1, \dots, τ_k) occur and the number of changepoints (k); the parameter λ controls the relative importance of these two terms.

The following result establishes an equivalence between (6) and (5).

PROPOSITION 1. *There is a one-to-one correspondence between the set of estimated spike events in the solution to (5) and the set of changepoints $0 = \tau_0, \tau_1, \dots, \tau_k, \tau_{k+1} = T$ in the solution to (6), in the sense that $\hat{c}_t \neq \gamma \hat{c}_{t-1}$ if and only if $t \in \{\tau_1 + 1, \dots, \tau_k + 1\}$. Furthermore, given the set of changepoints, the solution to (5) takes the form*

$$\hat{c}_t = \begin{cases} \gamma \hat{c}_{t-1} & \tau_j + 2 \leq t \leq \tau_{j+1}, \\ \frac{\sum_{t=\tau_j+1}^{\tau_{j+1}} y_t \gamma^{t-(\tau_j+1)}}{\sum_{t=\tau_j+1}^{\tau_{j+1}} \gamma^{2(t-(\tau_j+1))}} & t = \tau_j + 1, \end{cases}$$

for $j \in \{0, \dots, k\}$.

Proposition 1 indicates that in order to solve (5), it suffices to solve (6). We note that due to a slight discrepancy between the conventions used in the changepoint detection literature and the notion of a spike event in this paper, the indexing in Proposition 1 is a little bit awkward, in the sense that the k th spike event is estimated to occur at time $\tau_k + 1$, rather than at time τ_k .

In the next two sections, we will make use of the following result.

PROPOSITION 2. *The quantity (7) has a closed-form expression,*

$$\mathcal{D}(y_{a:b}) = \sum_{t=a}^b \frac{y_t^2}{2} - \mathcal{C}(y_{a:b}) \sum_{t=a}^b y_t \gamma^{t-a} + \frac{\mathcal{C}(y_{a:b})^2}{2} \sum_{t=a}^b \gamma^{2(t-a)}, \quad \text{where}$$

$$\mathcal{C}(y_{a:b}) = \frac{\sum_{t=a}^b y_t \gamma^{t-a}}{\sum_{t=a}^b \gamma^{2(t-a)}}.$$

Furthermore, given $\mathcal{D}(y_{a:b})$, we can calculate $\mathcal{D}(y_{a:(b+1)})$ in constant time.

Propositions 1 and 2 are proven in Appendix A.

2.2. *An algorithm for solving (5) in $\mathcal{O}(T^2)$ operations.* In this section we apply a dynamic programming algorithm proposed by Jackson et al. (2005) and Auger and Lawrence (1989) in order to solve the changepoint detection problem (6) for the global optimum in $\mathcal{O}(T^2)$ time. Due to the equivalence between (6) and (5) established in Proposition 1, this algorithm also solves problem (5).

Roughly speaking, this algorithm recasts the very difficult problem of choosing the times of all changepoints simultaneously into the much simpler problem of choosing the time of just the most recent changepoint. In greater detail consider

solving (6) on the first s timesteps. Define $F(0) \equiv -\lambda$, and for $s \geq 1$, define

$$\begin{aligned}
 F(s) &= \min_{0=\tau_0 < \tau_1 < \dots < \tau_k < \tau_{k+1}=s, k} \left\{ \sum_{j=0}^k \mathcal{D}(y(\tau_j+1):\tau_{j+1}) + \lambda k \right\} \\
 &= \min_{0=\tau_0 < \tau_1 < \dots < \tau_k < \tau_{k+1}=s, k} \left\{ \sum_{j=0}^k [\mathcal{D}(y(\tau_j+1):\tau_{j+1}) + \lambda] - \lambda \right\} \\
 (8) \quad &= \min_{0=\tau_0 < \tau_1 < \dots < \tau_k < \tau_{k+1}=s, k} \left\{ \sum_{j=0}^{k-1} [\mathcal{D}(y(\tau_j+1):\tau_{j+1}) + \lambda] - \lambda + \mathcal{D}(y(\tau_k+1):\tau_{k+1}) + \lambda \right\} \\
 &= \min_{0 \leq \tau_k < \tau_{k+1}=s} \left\{ \min_{0=\tau_0 < \tau_1 < \dots < \tau_{k'} < \tau_{k'+1}=\tau_k, k'} \left\{ \sum_{j=0}^{k'} [\mathcal{D}(y(\tau_j+1):\tau_{j+1}) + \lambda] - \lambda \right\} + \mathcal{D}(y(\tau_k+1):\tau_{k+1}) + \lambda \right\} \\
 &= \min_{0 \leq \tau < s} \{F(\tau) + \mathcal{D}(y(\tau+1):s) + \lambda\}.
 \end{aligned}$$

In other words, in order to solve (6) we need simply identify the time of the most recent changepoint, and then solve (6) on all earlier times.

This recursion gives a simple recipe for evaluating $F(T)$ efficiently; set $F(0) = -\lambda$ and compute $F(1), F(2), \dots, F(T)$ based on previously calculated (and stored) values. For example, at $s = 1$, calculate and store

$$F(1) = \min_{0 \leq \tau < 1} \{F(\tau) + \mathcal{D}(y(\tau+1):1) + \lambda\} = F(0) + \mathcal{D}(y_1) + \lambda,$$

and then at $s = 2$ use the previously calculated values $F(0)$ and $F(1)$ to compute the minimum over a finite set with s elements

$$\begin{aligned}
 F(2) &= \min_{\tau \in \{0,1\}} \{F(\tau) + \mathcal{D}(y(\tau+1):2) + \lambda\} \\
 &= \min\{F(0) + \mathcal{D}(y_{1:2}) + \lambda, F(1) + \mathcal{D}(y_2) + \lambda\}.
 \end{aligned}$$

Given $F(1), \dots, F(s - 1)$, computing $F(s)$ requires minimizing over a finite set of size s , and therefore it has computational cost linear in s . The total cost of computing $F(T)$ is quadratic in the total number of timesteps, T , since there are $T + 1$ subproblems, $\sum_{s=0}^T s = \mathcal{O}(T^2)$.

Full details are provided in Algorithm 1. We note that this algorithm is particularly efficient in light of Proposition 2, which makes it possible to perform a constant-time update to $\mathcal{D}(y(\tau+1):s)$ in order to compute $\mathcal{D}(y(\tau+1):(s+1))$.

2.3. Dramatic speedups using cost-complexity pruning. In a recent paper Killick, Fearnhead and Eckley (2012) considered problems of the form (6) for which an assumption on $\mathcal{D}(\cdot)$ holds; this assumption is satisfied by (7).

The main insight of their paper is as follows. Suppose that $s < r$ and $F(s) + \mathcal{D}(y_{(s+1):r}) > F(r)$. Then for any $q > r$, it is mathematically impossible for the most recent changepoint before the q th timestep to have occurred at the s th timestep. This allows us to *prune* the set of candidate changepoints that must be

Algorithm 1: An $\mathcal{O}(T^2)$ algorithm for solving (5)

Initialize: $F(0) = -\lambda$, $\text{cp}(0) = \emptyset$

1 **foreach** $s = 1, 2, \dots, T$ **do**

2 Calculate $F(s) = \min_{0 \leq \tau < s} \{F(\tau) + \mathcal{D}(y_{(\tau+1):s}) + \lambda\}$

3 Set $s' = \operatorname{argmin}_{0 \leq \tau < s} \{F(\tau) + \mathcal{D}(y_{(\tau+1):s}) + \lambda\}$

4 Update $\text{cp}(s) = (\text{cp}(s'), s')$

5 **end**

Output : The number of spike events $k \equiv \text{card}(\text{cp}(T))$, the changepoints $\{\tau_1, \dots, \tau_k\} \equiv \text{cp}(T)$, the spike times $\{\tau_1 + 1, \dots, \tau_k + 1\}$ and the estimated calcium concentrations

$$\hat{c}_t \equiv \begin{cases} \gamma \hat{c}_{t-1} & \tau_j + 2 \leq t \leq \tau_{j+1}, \\ \frac{\sum_{t=\tau_j+1}^{\tau_{j+1}} y_t \gamma^{t-(\tau_j+1)}}{\sum_{t=\tau_j+1}^{\tau_{j+1}} \gamma^{2(t-(\tau_j+1))}} & t = \tau_j + 1, \end{cases}$$

for $j = 0, \dots, k$, where $\tau_0 = 0$.

considered in each step of Algorithm 2, leading to drastic speedups. Details are provided in Algorithm 2, which solves (5) for the global optimum.

Under several technical assumptions Killick, Fearnhead and Eckley (2012) show that the expected complexity of this algorithm is $\mathcal{O}(T)$. The main assumption is that the expected number of changepoints in the data increases linearly with the length of the data; this is reasonable in the context of calcium imaging data, in which we expect the number of neuron spike events to be linear in the length of the recording.

2.4. Timing results for solving (5). We simulated data from (1) with $\gamma = 0.998$, $\sigma = 0.15$ and $s_t \sim_{\text{ind.}} \text{Poisson}(\theta)$ with $\theta \in \{0.1, 0.01, 0.001\}$. We solved (5) with $\lambda = 1$ using our R-language implementations of Algorithms 1 and 2.

Timing results, averaged over 50 simulated datasets, are displayed in Figure 2. As expected the running time of Algorithm 1 scales quadratically in the length of the time series, whereas the running time of Algorithm 2 is upper bounded by that of Algorithm 1. Furthermore, the running time of Algorithm 2 decreases as the firing rate increases. The Chen et al. (2013) dataset explored in Section 4.1 has firing rate on the same order of magnitude as the middle panel, $\theta = 0.01$. Using Algorithm 2, we can solve (5) for the global optimum in a few minutes on a 2.5 GHz Intel Core i7 Macbook Pro on fluorescence traces of length 100,000 with moderate to high firing rates.

We note here that Algorithm 2 for solving (5) is much slower than the algorithm of Friedrich, Zhou and Paninski (2017) for solving (3), which is implemented in

Algorithm 2: An algorithm for solving (5) in substantially fewer than $\mathcal{O}(T^2)$ operations

Initialize: $F(0) = -\lambda$, $\text{cp}(0) = \emptyset$, $\mathcal{E}_1 = \{0\}$

1 **foreach** $s = 1, 2, \dots, T$ **do**

2 Calculate $F(s) = \min_{\tau \in \mathcal{E}_s} \{F(\tau) + \mathcal{D}(y_{(\tau+1):s}) + \lambda\}$

3 Set $s' = \operatorname{argmin}_{\tau \in \mathcal{E}_s} \{F(\tau) + \mathcal{D}(y_{(\tau+1):s}) + \lambda\}$

4 Update $\mathcal{E}_{s+1} = \{\tau \in \{\mathcal{E}_s \cup s\} : F(\tau) + \mathcal{D}(y_{(\tau+1):s}) < F(s)\}$

5 Update $\text{cp}(s) = (\text{cp}(s'), s')$

6 **end**

Output : The number of spike events $k \equiv \text{card}(\text{cp}(T))$, the changepoints $\{\tau_1, \dots, \tau_k\} \equiv \text{cp}(T)$, the spike times $\{\tau_1 + 1, \dots, \tau_k + 1\}$, and the estimated calcium concentrations

$$\hat{c}_t \equiv \begin{cases} \gamma \hat{c}_{t-1} & \tau_j + 2 \leq t \leq \tau_{j+1}, \\ \frac{\sum_{t=\tau_j+1}^{\tau_{j+1}} y_t \gamma^{t-(\tau_j+1)}}{\sum_{t=\tau_j+1}^{\tau_{j+1}} \gamma^{2(t-(\tau_j+1))}} & t = \tau_j + 1, \end{cases}$$

for $j = 0, \dots, k$, where $\tau_0 = 0$.

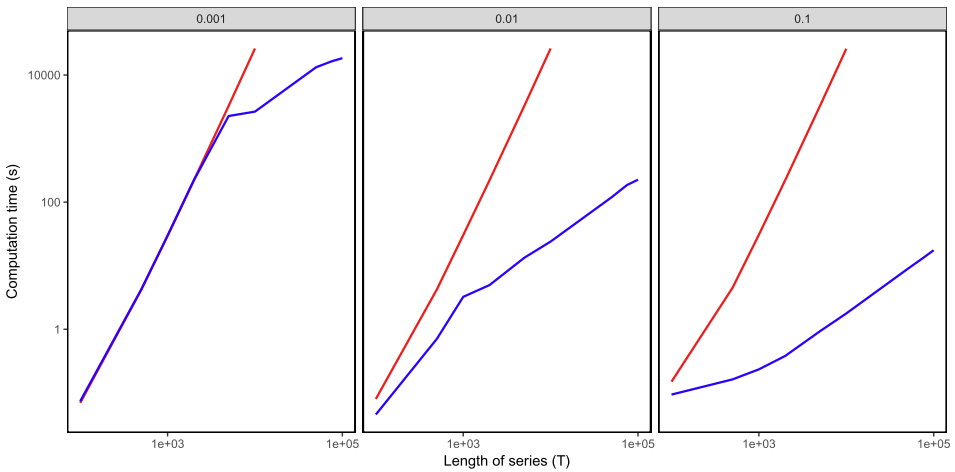


FIG. 2. Timing results for solving (5) for the global optimum, using Algorithms 1 (—) and 2 (—). The x-axis displays the length of the time series (T), and the y-axis displays the average running time in seconds. Each panel, from left to right, corresponds to data simulated according to (1) with $s_t \sim \text{i.i.d. Poisson}(\theta)$, with $\theta \in \{0.001, 0.01, 0.1\}$. Standard errors are on average $< 0.1\%$ of the mean compute time. Additional details are provided in Section 2.4.

Cython and has approximately linear running time. It should be possible to develop a faster algorithm for solving (5) using ideas from Johnson (2013), Maidstone et al. (2017) and Hocking et al. (2017). Furthermore, a much faster implementation of Algorithm 2 would be possible using a language other than R. We leave such improvements to future work.

3. Simulation study.

3.1. *Comparison methods.* In this section, we use *in silico* data to demonstrate the performance advantages of the ℓ_0 approach (5) over two competing approaches:

1. The ℓ_1 proposal (3) of Friedrich and Paninski (2016) and Friedrich, Zhou and Paninski (2017), which involves a single tuning parameter λ .

2. A thresholded version of the ℓ_1 estimator. Letting $\hat{s}_2, \dots, \hat{s}_T$ denote the solution to (3), we define the *post-thresholding estimator* as

$$(9) \quad \tilde{s}_t = \hat{s}_t 1_{(\hat{s}_t \geq L)}, \quad t = 2, \dots, T,$$

for L a positive constant. In other words the post-thresholding estimator retains only the estimated spikes for which the estimated increase in calcium exceeds a threshold L . The post-thresholding estimator involves two tuning parameters— λ in (3), as well as the value of L used to perform thresholding.

The post-thresholding estimator is motivated by the fact that the solution to (3) tends to yield many “small” spikes, that is, \hat{s}_t is near zero, but not exactly equal to zero, for many timesteps. In fact this can be seen in Figure 1(c). As seen in Figure 1(e), the post-thresholding estimator has the potential to improve the performance of the ℓ_1 estimator by removing some of these small spikes. Of course, the post-thresholding estimator with $L = 0$ is identical to the ℓ_1 estimator from (3).

3.2. *Performance measures.* We measure performance of each method based on two criteria: (i) error in calcium estimation and (ii) error in spike detection.

We consider the mean of squared differences between the true calcium concentration in (1) and the estimated calcium concentration that solves (5),

$$(10) \quad \text{MSE}(c, \hat{c}) = \frac{1}{T} \sum_{t=1}^T (c_t - \hat{c}_t)^2.$$

This quantity involves the unobserved calcium concentrations, c_1, \dots, c_T , and thus can only be computed on simulated data. Furthermore, this quantity can be computed for our ℓ_0 proposal (5) and for the ℓ_1 proposal (3) but not for the post-thresholding estimator (9), since the post-thresholding estimator does not lead to an estimate of the underlying calcium concentrations.

We now consider the task of quantifying the error in spike detection. We make use of the Victor–Purpura distance metric [Victor and Purpura (1996, 1997)], which defines the distance between two spike trains as the minimum cost of transforming one spike train to the other through spike insertion, deletion or translation. We also use the van Rossum distance [van Rossum (2001)], defined as the mean squared difference between two spike trains that have been convolved with an exponential kernel with timescale $\tau = 2$.

3.3. Results. We generated 100 simulated datasets according to (1) with parameter settings $\gamma = 0.96$, $T = 5000$, $\sigma = 0.15$ and $s_t \sim_{\text{i.i.d.}} \text{Poisson}(0.01)$.

On each simulated dataset we solved (5) and (3) for a range of values of the tuning parameter λ . Moreover, we post-thresholded the ℓ_1 solution, as in (9), with five different threshold values: $L \in \{0, 0.125, 0.250, 0.375, 0.500\}$.

Figure 3(a) displays the error in spike event detection for the van Rossum distance, Figure 3(b) displays the error in spike event detection for the Victor–Purpura distance metric and Figure 3(c) displays the error in calcium estimation (10), for the ℓ_0 problem (5) and the ℓ_1 problem (3), for a range of values of λ . Results are averaged over the 50 simulated datasets.

As mentioned earlier, since the calcium concentration is not defined for the post-thresholding estimator (9), the post-thresholding estimator is not displayed in Figure 3(c). In Figures 3(a) and 3(b), five distinct curves are displayed for the post-thresholding operator; each corresponds to a distinct value of L . Note that as L increases, the maximum possible number of estimated spikes from the post-thresholding estimator decreases. For example, with $\lambda = 0$ and $L = 0.5$, no more than approximately 50 spikes are estimated by the post-thresholding estimator. For this reason some of the curves corresponding to the post-thresholding estimator appear truncated in Figures 3(a) and 3(b).

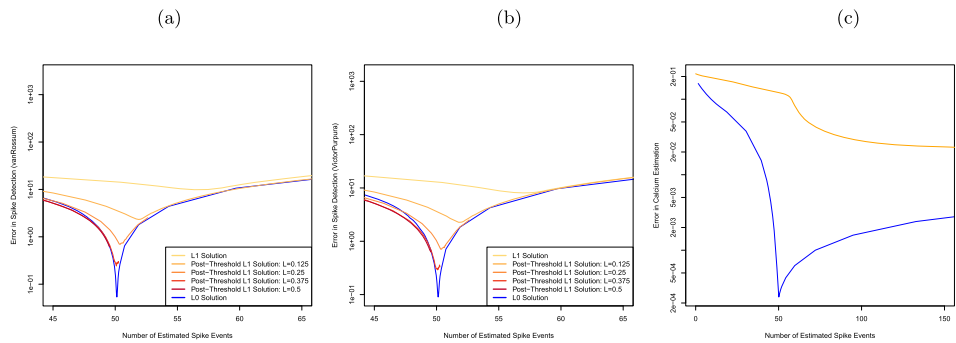


FIG. 3. Simulation study to assess the error in spike detection and calcium estimation, for the ℓ_1 (3), post-thresholded ℓ_1 (9) and ℓ_0 (4) problems. (a): Error in spike detection measured using van Rossum distance. (b): Error in spike detection, measured using Victor-Purpura distance. (c): Error in calcium estimation (10). Simulation details are provided in Section 3.

Figure 3 reveals that the ℓ_0 estimator (5) results in dramatically lower errors in both calcium estimation and spike detection than the ℓ_1 estimator (3) (which is equivalent to the post-thresholding operator with $L = 0$). Although post-thresholding with $L > 0$ improves upon the unthresholded ℓ_1 estimator, the ℓ_0 estimator still substantially outperforms all competitors in Figures 3(a) and 3(b). Moreover, the ℓ_0 estimator requires just a single tuning parameter λ in (5), whereas the post-thresholding procedure involves two tuning parameters, λ in (3) and L in (9), leading to challenges in tuning parameter selection.

Furthermore, the ℓ_0 problem (5) achieves the lowest errors in both calcium estimation and spike detection when applied using a value of the tuning parameter λ that yields approximately 50 estimated spikes, which is the expected number of spikes in this simulation. This suggests that it should be possible to use a cross-validation scheme to select the tuning parameter λ for the ℓ_0 approach; we propose such a scheme in Appendix B. By contrast in Figure 3(b), the ℓ_1 approach achieves its lowest error in calcium estimation when far more than 50 spikes are estimated. This is a consequence of the fact that the ℓ_1 penalty simultaneously reduces the number of estimated spikes and shrinks the estimated calcium. Therefore, the value of the tuning parameter λ in (3) that yields the most accurate estimate of calcium will result in severe over-estimation of the number of spikes. This means that the cross-validation scheme detailed in Appendix B will not perform well for the ℓ_1 approach.

4. Application to calcium imaging data. In this section we apply our ℓ_0 proposal (5) and the ℓ_1 proposal of Friedrich and Paninski (2016) and Friedrich, Zhou and Paninski (2017) (3), both with and without post-thresholding (9) to two calcium imaging datasets. In the first dataset, the true spike times are known [Chen et al. (2013), GENIE Project (2015)], and so we can directly assess the spike detection accuracy of each proposal. In the second dataset the true spike times are unknown [Allen Institute for Brain Science (2016), Hawrylycz et al. (2016)]; nonetheless, we are able to make a qualitative comparison of the results of the ℓ_1 and ℓ_0 proposals.

4.1. Application to Chen et al. (2013) data. We first consider a dataset that consists of simultaneous calcium imaging and electrophysiological measurements [Chen et al. (2013), GENIE Project (2015)], obtained from the Collaborative Research in Computational Neuroscience portal (<http://crcns.org/data-sets/methods/cai-1/about-cai-1>). In what follows we refer to the spike times inferred from the electrophysiological measurements as the “true” spikes.

The top panel of Figure 4 shows a 40-second recording from cell 2002, which expresses GCaMP6s. The data are measured at 60 Hz for a total of 2400 timesteps. The raw fluorescence traces are DF/F transformed with a 20% percentile filter as in Figure 3 of Friedrich, Zhou and Paninski (2017). In this 40-second recording there are a total of 23 true spikes; therefore, we solved the ℓ_0 and ℓ_1 problems with

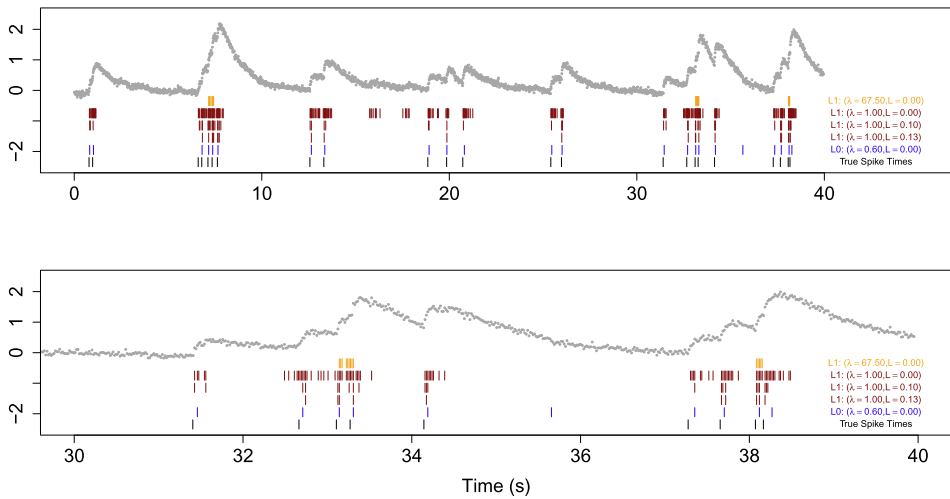


FIG. 4. Spike detection for cell 2002 of the *Chen et al. (2013)* data. The observed fluorescence (\bullet) and true spikes (—) are displayed. Estimated spike times from the ℓ_0 problem (4) are shown in (—), estimated spike times from the ℓ_1 problem (3) are shown in (—), and estimated spike times from the post-thresholding estimator (9) are shown in (—). Times 0s–35s are shown in the top row; the second row zooms into time 30s–40s in order to illustrate the behavior around a large increase in calcium concentration.

$\gamma = 0.9864405$ using values of λ in (5) and (3) that yield 23 estimated spikes. Additionally, we solved the ℓ_1 problem with $\lambda = 1$ and post-thresholded it according to (9) using $L = 0, 0.1$, and 0.13 ; these threshold values yielded 230, 54, and 23 estimated spikes, respectively.

Figure 4 displays the estimated spikes resulting from the ℓ_0 proposal, the estimated spikes resulting from the ℓ_1 proposal, the estimated spikes from post-thresholding the ℓ_1 solutions, and the ground truth spikes. We see that the ℓ_0 proposal has one false negative (i.e., it misses one true spike at around 7 seconds) and one false positive (i.e., it estimates a spike at around 36 seconds, where there is no true spike). By contrast, the ℓ_1 problem concentrates the 23 estimated spikes at three points in time, and therefore suffers from a substantial number of false positives as well as false negatives. Because the ℓ_1 penalty controls both the number of spikes and the estimated calcium, the ℓ_1 problem tends to put a large number of spikes in a row, each of which is associated with a very modest increase in calcium. This is consistent with the results seen in Figures 1 and 3. Post-thresholding the ℓ_1 estimator does lead to an improvement in results relative to the unthresholded ℓ_1 method; however, the post-thresholded solution with 23 spikes still tends to estimate a number of spikes in short succession when in fact only one true spike is present, and also misses several true spike events.

We note that the ℓ_0 method tends to estimate spike times one or two timesteps ahead of the true spike times. This is due to model misspecification. Model (1)

with $p = 1$ assumes that the calcium concentration increases instantaneously due to a spike event and subsequently decays; however, we see from Figure 4 that in reality, a spike event is followed by an increase in calcium over the course of a few timesteps before the onset of exponential decay. We see two possible avenues to address this relatively minor issue: estimated spike times from the ℓ_0 method can be adjusted to account for this empirical observation; or else the optimization problem (5) can be adjusted in order to allow for more realistic calcium dynamics [e.g., by solving an ℓ_0 optimization problem corresponding to (1) with $p > 1$]. We explore the second alternative in Section 5.

In Appendix C we apply an approach proposed by Friedrich, Zhou and Paninski (2017) to approximate the solution to a nonconvex problem using a greedy algorithm. This alternative approach performs quite a bit better than solving the ℓ_1 problem (3); however, it does not achieve the global optimum.

4.2. Application to Allen brain observatory data. We now consider a dataset from the Allen Brain Observatory, a large open-source repository of calcium imaging data from the mouse visual cortex [Allen Institute for Brain Science (2016), Hawrylycz et al. (2016)]. For this data the true spike times are not available, and so it is difficult to objectively assess the performances of the ℓ_1 , post-thresholded ℓ_1 , and ℓ_0 methods. Instead, for each method we present several fits that differ in the number of detected spikes. We argue that the ℓ_0 problem yields results that are qualitatively superior to those of the competitors, in the sense that they are better supported by visual inspection of the data.

For the second ROI in NWB 510221121, we applied the ℓ_1 , post-thresholded ℓ_1 , and ℓ_0 methods to the first 10,000 timesteps of the DF/F -transformed fluorescence traces. Since the data are measured at 30 Hz, this amounts to the first 333 seconds of the recording. Figure 5 shows the results obtained with $\gamma = 0.981756$.

For the ℓ_0 and ℓ_1 estimators we chose the values of λ in (3) and (5) in order to obtain 27, 49 and 128 estimated spikes. For the post-thresholded estimator (9) we set $\lambda = 1$, and then selected L to yield 27, 49 and 128 estimated spikes.

As in the previous subsection we see that, when faced with a large increase in fluorescence, the ℓ_1 problem tends to estimate a very large number of spikes in quick succession. For example, when 27 spikes are estimated, the ℓ_1 problem concentrates the estimated spikes at three points in time [Figure 5(a)]. Even when 128 spikes are estimated, the ℓ_1 problem still seems to miss all but the largest peaks in the fluorescence data [Figure 5(c)]. Post-thresholding the ℓ_1 estimator improves upon this issue somewhat, but spikes corresponding to smaller increases in fluorescence are still missed; this issue can be clearly seen in Figures 5(d)–(f), which zoom in on a smaller time window.

By contrast the ℓ_0 problem can assign an arbitrarily large increase in calcium to a single spike event. Therefore, it seems to capture most of the visible peaks in the fluorescence data when 49 spikes are estimated [Figures 5(b) and 5(e)], and it captures all of them when 128 spikes are estimated [Figures 5(c) and 5(f)].

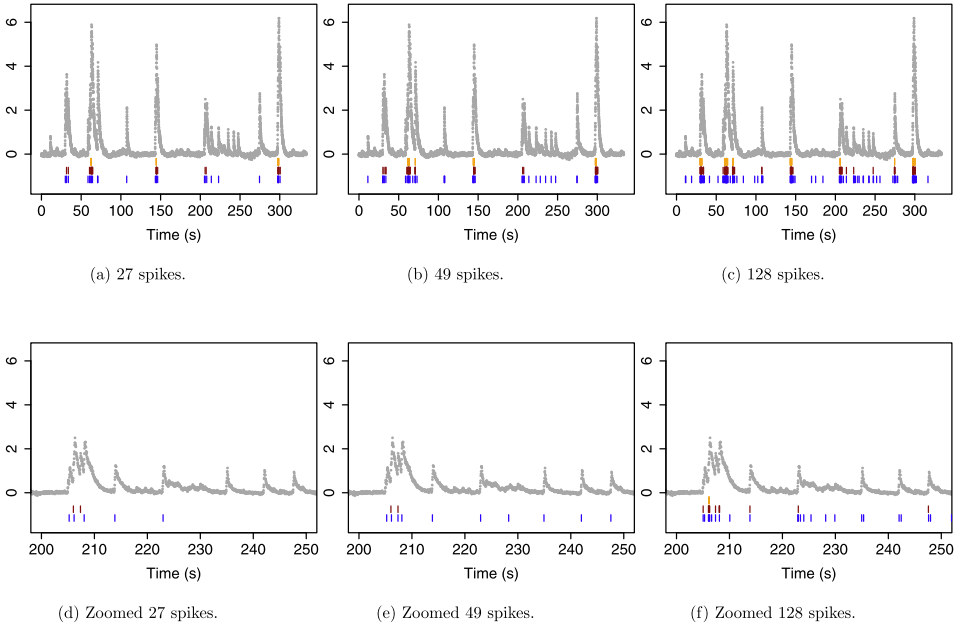


FIG. 5. *The first 10,000 timesteps from the second ROI in NWB 510221121 from the Allen Brain Observatory. Each panel displays the Df/F-transformed fluorescence (\bullet), the estimated spikes from the ℓ_0 problem (—) (5), the estimated spikes from the ℓ_1 problem (—) (3), and the estimated spikes from post-thresholding the ℓ_1 problem (—) (9). The panels display results from applying the ℓ_1 and ℓ_0 methods with tuning parameter λ chosen to yield (a): 27 spikes for each method; (b): 49 spikes for each method; and (c): 128 spikes for each method. The post-thresholding estimator was obtained by applying the ℓ_1 method with $\lambda = 1$, and thresholding the result to obtain 27, 49 or 128 spikes. (d)–(f): As in (a)–(c), but zoomed in on 200–250 seconds.*

Though the true spike times are unknown for this data, based on visual inspection, the results for the ℓ_0 proposal seem superior to those of the ℓ_1 and post-thresholded ℓ_1 proposals.

5. Extensions. We now present two straightforward extensions to the optimization problem (5) for which computationally attractive algorithms along the lines of the one proposed in Section 2 are available.

5.1. Estimation of the intercept in (1). The model for calcium dynamics considered in this paper (1) allows for an intercept term, β_0 . In order to arrive at (5) we assumed that the intercept was known and (without loss of generality) equal to zero. However, in practice we might want to fit the model (1) without knowing the value of the intercept β_0 . In fact, in many settings this may be of great practical importance, since the meaning of the model (1) (and, for instance, the rate of exponential decay γ) is inextricably tied to the value of the intercept.

We now propose a modification to the ℓ_0 optimization problem (5) that allows for estimation of the intercept β_0 . So that the resulting problem can be efficiently solved using the ideas laid out in Section 2, we must ensure that given the estimated spike times, the calcium can be estimated separately between each pair of consecutive spikes. Consequently, we must allow for a separate intercept term between each pair of consecutive spikes. This suggests the optimization problem

$$(11) \quad \underset{c_1, \dots, c_T, \beta_{01}, \dots, \beta_{0T}}{\text{minimize}} \left\{ \frac{1}{2} \sum_{t=1}^T (y_t - c_t - \beta_{0t})^2 + \lambda \sum_{t=2}^T 1_{(c_t \neq \gamma c_{t-1}, \beta_{0t} \neq \beta_{0,t-1})} \right\},$$

where the indicator variable $1_{(A, B)}$ equals one if the event $A \cup B$ holds, and equals zero otherwise. Therefore, $1_{(c_t \neq \gamma c_{t-1}, \beta_{0t} \neq \beta_{0,t-1})}$ equals *one* if the calcium concentration stops decaying or if the intercept changes. Note that in the solution to (11), the intercept is constant between adjacent timesteps, unless there is a spike.

Problem (11) can be recast as a changepoint problem of the form (6) with

$$\mathcal{D}(y_{a:b}) \equiv \min \left\{ \frac{1}{2} \sum_{t=a}^b (y_t - c_t - \beta_{0t})^2 \right\}$$

subject to $c_t = \gamma c_{t-1}, \beta_{0t} = \beta_{0,t-1}, \quad t = a + 1, \dots, b.$

Given $\mathcal{D}(y_{a:b}), \mathcal{D}(y_{a:(b+1)})$ can be updated in constant time. Thus, the algorithms introduced in Section 2 can be easily modified in order to solve (11) for the global optimum.

5.2. An autoregressive model with $p > 1$ in (1). The model (1) allows for the calcium dynamics to follow a p th order autoregressive process. For simplicity this paper focused on the case of $p = 1$. We now consider developing an ℓ_0 optimization problem for the model (1) with $p > 1$.

It is natural to consider the ℓ_0 optimization problem

$$(12) \quad \underset{c_1, \dots, c_T}{\text{minimize}} \left\{ \frac{1}{2} \sum_{t=1}^T (y_t - c_t)^2 + \lambda \sum_{t=p+1}^T 1_{(c_t \neq \sum_{i=1}^p \gamma_i c_{t-i})} \right\}.$$

However, (12) cannot be expressed in the form (6). The penalty in (12) induces a dependency in the calcium that spans more than two timesteps, so that the calcium at a given timestep may depend on the calcium prior to the most recent spike. As a result (12) is computationally intractable.

Instead, we consider a changepoint detection problem of the form (6) with cost function

$$\mathcal{D}(y_{a:b}) \equiv \min \left\{ \frac{1}{2} \sum_{t=a}^b (y_t - c_t)^2 \right\}$$

subject to $c_t = \sum_{i=1}^p \gamma_i c_{t-i}, \quad t = a + p, \dots, b.$

Thus, the calcium follows a p th order autoregressive model between any pair of spikes; furthermore, once a spike occurs, the calcium concentrations are reset completely. That is, the calcium after a spike is not a function of the calcium before a spike. Consequently, it is straightforward to develop a fast algorithm for solving this changepoint detection problem for the global optimum using ideas detailed in Section 2.

In particular a popular model for calcium dynamics assumes that, between any pair of spikes, the calcium can be well approximated by the difference between two exponentially-decaying functions [Brunel and Wang (2003), Cavallari, Panzeri and Mazzoni (2016), Mazzoni et al. (2008), Volgushev, Ilin and Stevenson (2015)]. This would perhaps be a better model for the data from the Allen Brain Observatory, in which increases in fluorescence due to a spike occur over the course of a few timesteps rather than instantaneously; see Figure 5. This “difference of exponentials” model falls directly within the framework of (1) with $p = 2$, and hence could be handled using the changepoint detection problem just described.

6. Discussion. In this paper, we considered solving the seemingly intractable ℓ_0 optimization problem (5) corresponding to the model (1). By recasting (5) as a changepoint detection problem, we were able to derive an algorithm to solve (5) for the global optimum in expected linear time. It should be possible to develop an even more efficient algorithm for solving (5) that exploits recent algorithmic developments for changepoint detection [Johnson (2013), Maidstone et al. (2017), Hocking et al. (2017)]; we leave this as an avenue for future work.

We have shown in this paper that solving the ℓ_0 optimization problem (5) leads to more accurate spike event detection than solving the ℓ_1 optimization problem (3) proposed by Friedrich, Zhou and Paninski (2017). Indeed, this finding is intuitive: the ℓ_1 penalty and positivity constraint in (3) serves as an exponential prior on the increase in calcium at any given time point and thereby effectively limits the amount that calcium can increase in response to a spike event. By contrast the ℓ_0 penalty in (5) is completely agnostic to the amount by which a spike event increases the level of calcium. Consequently, it can allow for an arbitrarily large (or small) increase in fluorescence as a result of a spike event.

While approximations to the solution to the ℓ_0 problem (5) are possible [de Rooi and Eilers (2011), de Rooi, Ruckebusch and Eilers (2014), Hugelier et al. (2016), Scott and Knott (1974), Olshen et al. (2004), Fryzlewicz (2014), Friedrich, Zhou and Paninski (2017)], there is no guarantee that such approaches will yield an attractive local optimum on a given dataset. In this paper we completely bypass this concern by solving the ℓ_0 problem for the global optimum.

In this paper we have focused on the empirical benefits of the ℓ_0 problem (5) over the ℓ_1 problem (3). However, it is natural to wonder whether these empirical benefits are backed by statistical theory. Conveniently, both the ℓ_0 and ℓ_1 optimization problems are very closely related to problems that have been well studied in the statistical literature from a theoretical standpoint. In particular, in the special

case of $\gamma = 1$, the ℓ_0 problem (5) was extensively studied in Yao and Au (1989) and Boysen et al. (2009). Furthermore, when $\gamma = 1$, the ℓ_1 problem (5) is very closely related to the *fused lasso* optimization problem,

$$\underset{c_1, \dots, c_T}{\text{minimize}} \left\{ \frac{1}{2} \sum_{t=1}^T (y_t - c_t)^2 + \lambda \sum_{t=2}^T |c_t - c_{t-1}| \right\},$$

which has also been extremely well studied [Tibshirani et al. (2005), Mammen and van de Geer (1997), Davies and Kovac (2001), Rinaldo (2009), Harchaoui and Lévy-Leduc (2010), Qian and Jia (2012), Rojas and Wahlberg (2014), Lin et al. (2016), Dalalyan, Hebiri and Lederer (2017)]. However, we leave a formal theoretical analysis of the relative merits of (5) and (3), in terms of ℓ_2 error bounds and spike recovery properties, to future work.

Our R-language software for our proposal is available on CRAN in the package `LZeroSpikeInference`. Instructions for running this software in `python` can be found at <https://github.com/jewellsean/LZeroSpikeInference>.

APPENDIX A: PROOF OF PROPOSITIONS

A.1. Proof of Proposition 1. The first sentence follows by inspection. To establish the second sentence, we observe that the cost

$$\mathcal{D}(y_{a:b}) \equiv \min_{c_a, c_t = \gamma c_{t-1}, t=a+1, \dots, b} \left\{ \frac{1}{2} \sum_{t=a}^b (y_t - c_t)^2 \right\}$$

can be rewritten by direct substitution of the constraint as

$$\mathcal{D}(y_{a:b}) = \min_{c_a} \left\{ \frac{1}{2} \sum_{t=a}^b (y_t - \gamma^{t-a} c_a)^2 \right\}.$$

This is a least squares problem and is minimized at

$$\hat{c}_a = \frac{\sum_{t=a}^b y_t \gamma^{t-a}}{\sum_{t=a}^b \gamma^{2(t-a)}},$$

which implies that

$$\mathcal{D}(y_{a:b}) = \frac{1}{2} \sum_{t=a}^b (y_t - \gamma^{t-a} \hat{c}_a)^2,$$

and furthermore that for $a < t \leq b$ the fitted values are $\hat{c}_t = \gamma \hat{c}_{t-1}$. Applying this argument to each segment gives the result stated in Proposition 1.

A.2. Proof of Proposition 2. The first equation follows by expanding the square for the final form of $\mathcal{D}(y_{a:b})$ in the proof of Proposition 1. Given $\mathcal{D}(y_{a:b})$ we can calculate $\mathcal{D}(y_{a:(b+1)})$ in constant time by storing $\sum_{t=a}^b \frac{y_t^2}{2}$ and $\sum_{t=a}^b y_t \gamma^{t-a}$, and updating each of these sums for the new data point y_{b+1} ; we use a closed form expression to calculate $\sum_{t=a}^{b+1} \gamma^{2(t-a)}$. With each of these quantities stored, $\mathcal{D}(\cdot)$ and $\mathcal{C}(\cdot)$ are updated in constant time.

APPENDIX B: CHOOSING λ AND γ

Recall that in (5), the parameters λ and γ are unknown. The nonnegative parameter λ controls the tradeoff between the number of estimated spike events and the quality of the estimated calcium fit to the observed fluorescence. The parameter γ , $0 < \gamma < 1$, controls the rate of exponential decay of the calcium. We consider two approaches for choosing γ and λ .

B.1. Approach 1. To estimate γ , we manually select a segment $y_{a:b}$ that, based on visual inspection, appears to exhibit exponential decay. We then estimate γ as

$$\hat{\gamma} = \underset{\gamma}{\operatorname{argmin}} \{ \mathcal{D}(y_{a:b}) \} = \underset{\gamma}{\operatorname{argmin}} \left\{ \min_{c_a, c_t = \gamma c_{t-1}, t=a+1, \dots, b} \left\{ \frac{1}{2} \sum_{t=a}^b (y_t - c_t)^2 \right\} \right\}.$$

This can be done via numerical optimization.

Next, given γ , we select λ via cross-validation. For each value of λ that we consider, we solve (6) on a training set, and then evaluate the mean squared error (MSE) on a hold-out set. Details are provided in Algorithm 3.

B.2. Approach 2. Pnevmatikakis et al. (2013), Friedrich and Paninski (2016), and Friedrich, Zhou and Paninski (2017) propose to select the exponential decay parameter γ based on the autocovariance function, and to choose the tuning parameter λ such that $\|y - \hat{c}\|_2 \leq \sigma \sqrt{T}$, where the standard deviation σ is estimated through the power spectral density of y , and T is the number of timepoints. We refer the reader to Friedrich, Zhou and Paninski (2017) and Pnevmatikakis et al. (2016) for additional details.

APPENDIX C: A GREEDY APPROACH FOR APPROXIMATING THE SOLUTION TO A NONCONVEX PROBLEM

Friedrich, Zhou and Paninski (2017) consider a variant of the optimization problem (3),

$$(13) \quad \underset{c_1, \dots, c_T, s_2, \dots, s_T}{\operatorname{minimize}} \left\{ \frac{1}{2} \sum_{t=1}^T (y_t - c_t)^2 \right\}$$

subject to $s_t = c_t - \gamma c_{t-1} \geq s_{\min}$ or $s_t = 0$,

obtained from (3) by setting $\lambda = 0$, and changing the convex positivity constraint to the nonconvex constraint that s_t lies within a nonconvex set. Like (5), (13) is nonconvex. Friedrich, Zhou and Paninski (2017) do not attempt to solve (13) for the global optimum; instead, they provide a heuristic modification to their algorithm for solving (5), which is intended to approximate the solution to (13).

Figure 6 illustrates the behavior of this approximate algorithm when applied to the same data as in Figure 4. We set $\gamma = 0.9864405$, and considered three values

Algorithm 3: A cross-validation scheme for choosing λ (5)

Initialize: Candidate tuning parameter values $\lambda_1, \dots, \lambda_M$; a fixed value γ for the rate of exponential decay; a matrix $\text{cvMSE} \in \mathbb{R}^{M \times 2}$ to store the cross-validated MSEs.

1 **foreach** *fold* in 1, 2 **do**

2 Assign odd timesteps to the training set and even timesteps to the test set for the first fold, and vice-versa for the second fold. Note that $\text{card}(y^{\text{train}}) = \text{card}(y^{\text{test}}) = T/2$.

3 **foreach** $m = 1, \dots, M$ **do**

4 Solve (6) on the training set y^{train} with tuning parameter values λ_m and γ^2 , in order to obtain an estimate of the changepoints τ_1, \dots, τ_k . Set $\tau_0 = 0$ and $\tau_{k+1} = T/2$.

5 Average adjacent fitted values in order to obtain predictions on the test set y^{test} ,

$$\hat{c}^{\text{test}} = \frac{\hat{c}_{1:(T/2-1)}^{\text{train}} + \hat{c}_{2:(T/2)}^{\text{train}}}{2}.$$

6 Calculate and store the test set MSE,

$$\text{cvMSE}_{m,\text{fold}} = \frac{2}{T} \sum_{t=1}^{T/2} (y_t^{\text{test}} - \hat{c}_t^{\text{test}})^2.$$

7 **end**

8 **end**

9 Average the test set MSE over folds,

$$\overline{\text{cvMSE}}_m = \frac{1}{2} (\text{cvMSE}_{m,1} + \text{cvMSE}_{m,2}),$$

10 Calculate $\hat{m} = \text{argmin}_m \{\overline{\text{cvMSE}}_m\}$.

11 Calculate the standard error of the test set MSE over folds,

$$\text{se}(\text{cvMSE})_m = \sqrt{\frac{(\text{cvMSE}_{m,1} - \overline{\text{cvMSE}}_m)^2 + (\text{cvMSE}_{m,2} - \overline{\text{cvMSE}}_m)^2}{2}}$$

for $m = 1, \dots, M$.

12 Calculate

$$m^* = \max\{m : \overline{\text{cvMSE}}_m \leq \overline{\text{cvMSE}}_{\hat{m}} + \text{se}(\text{cvMSE})_{\hat{m}}\}.$$

Output : The value $\lambda_{\hat{m}}$ that minimize the cross-validated MSE, and the values λ_{m^*} selected based on the one-standard-error rule [Hastie, Tibshirani and Friedman (2009)].

of s_{\min} . When $s_{\min} = 10^{-8}$ and $s_{\min} = 0.1$, in panels (a) to (b), too many spikes are estimated. But when $s_{\min} = 0.3$, in panel (c), the solution to (13) is very similar to the solution to (5) with $\lambda = 0.6$. Both almost perfectly recover the ground truth spikes. Therefore, in this example, the approximate algorithm of Friedrich, Zhou and Paninski (2017) for solving (13) performs quite well.

However, (13) is a nonconvex problem, and the approximate algorithm of Friedrich, Zhou and Paninski (2017) is not guaranteed to find the global minimum. In fact, we can see that on the data shown in Figure 6, this approximate algorithm does not find the global optimum. When applied with $s_{\min} = 0.3$, the approximate algorithm yields an objective value of 8.57. By contrast, our algorithm for solving (5) yields a solution that is feasible for (13), and which results in a value of 7.86 for the objective of (13). We emphasize that this is quite remarkable: even though the algorithm proposed in Section 2 solves (5) and not (13), it *nonetheless yields a solution that is closer to the global optimum of (13) than does the approximate algorithm of Friedrich, Zhou and Paninski (2017), which is intended to solve (13)*.

In many cases, the greedy algorithm of Friedrich, Zhou and Paninski (2017) for solving (13) might yield good results that are near the global optimum of (13), and potentially even near the global optimum of (5). However, there is no guarantee

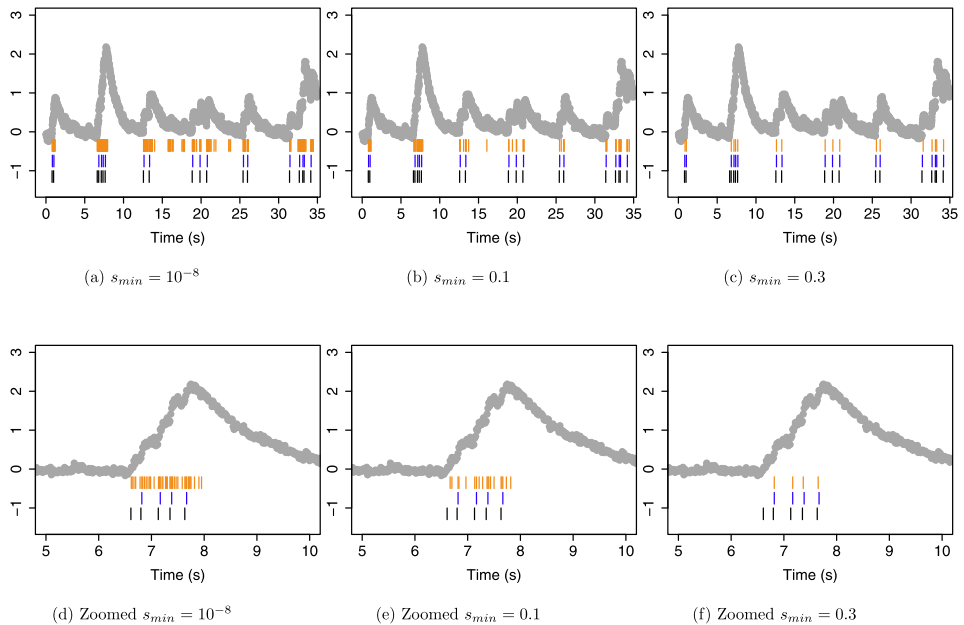


FIG. 6. Spike detection for cell 2002 of the Chen et al. (2013) data. In each panel, the observed fluorescence (\bullet) and true spikes (—) are displayed. Estimated spikes from problem (13) are shown in (—), and the estimated spikes from the ℓ_0 problem (5) with $\lambda = 0.6$ are shown in (—). Times 0 s–35 s are shown in the top row; the second row zooms in on times 5 s–10 s to illustrate behavior around a large increase in calcium concentration. Columns correspond to different values of s_{\min} .

that this algorithm will yield a “good” local optimum on any given dataset. By contrast, in this paper we have proposed an elegant and efficient algorithm for exactly solving the ℓ_0 problem (5).

Acknowledgments. We are grateful to three reviewers and an associate editor for helpful comments that improved the quality of this work. We thank Michael Buice and Kyle Lepage at the Allen Institute for Brain Science for conversations that motivated this work. Johannes Friedrich at Columbia University provided assistance in using his software to solve the ℓ_1 problem (3).

REFERENCES

- AHRENS, M. B., ORGER, M. B., ROBSON, D. N., LI, J. M. and KELLER, P. J. (2013). Whole-brain functional imaging at cellular resolution using light-sheet microscopy. *Nat. Methods* **10** 413–420.
- ALLEN INSTITUTE FOR BRAIN SCIENCE (2016). Stimulus set and response analysis. Technical report, Allen Institute, Seattle, WA.
- AUE, A. and HORVÁTH, L. (2013). Structural breaks in time series. *J. Time Series Anal.* **34** 1–16. [MR3008012](#)
- AUGER, I. E. and LAWRENCE, C. E. (1989). Algorithms for the optimal identification of segment neighborhoods. *Bull. Math. Biol.* **51** 39–54. [MR0978902](#)
- BIEN, J. and WITTEN, D. (2016). Penalized estimation in complex models. In *Handbook of Big Data*. 285–303. CRC Press, Boca Raton, FL. [MR3674823](#)
- BOYD, S. and VANDENBERGHE, L. (2004). *Convex Optimization*. Cambridge Univ. Press, Cambridge. [MR2061575](#)
- BOYSEN, L., KEMPE, A., LIEBSCHER, V., MUNK, A. and WITTICH, O. (2009). Consistencies and rates of convergence of jump-penalized least squares estimators. *Ann. Statist.* **37** 157–183. [MR2488348](#)
- BRAUN, J. V. and MÜLLER, H.-G. (1998). Statistical methods for DNA sequence segmentation. *Statist. Sci.* **13** 142–162.
- BRUNEL, N. and WANG, X.-J. (2003). What determines the frequency of fast network oscillations with irregular neural discharges? I. Synaptic dynamics and excitation-inhibition balance. *J. Neurophysiol.* **90** 415–430.
- CAVALLARI, S., PANZERI, S. and MAZZONI, A. (2016). Comparison of the dynamics of neural interactions between current-based and conductance-based integrate-and-fire recurrent networks. *Frontiers in Neural Circuits* **8**.
- CHEN, T.-W., WARDILL, T. J., SUN, Y., PULVER, S. R., RENNINGER, S. L., BAOHAN, A., SCHREITER, E. R., KERR, R. A., ORGER, M. B., JAYARAMAN, V. et al. (2013). Ultrasensitive fluorescent proteins for imaging neuronal activity. *Nature* **499** 295–300.
- DALALYAN, A. S., HEBIRI, M. and LEDERER, J. (2017). On the prediction performance of the Lasso. *Bernoulli* **23** 552–581. [MR3556784](#)
- DAVIES, P. L. and KOVAC, A. (2001). Local extremes, runs, strings and multiresolution. *Ann. Statist.* **29** 1–65. [MR1833958](#)
- DAVIS, R. A., LEE, T. C. M. and RODRIGUEZ-YAM, G. A. (2006). Structural break estimation for nonstationary time series models. *J. Amer. Statist. Assoc.* **101** 223–239. [MR2268041](#)
- DE ROOI, J. and EILERS, P. (2011). Deconvolution of pulse trains with the L_0 penalty. *Anal. Chim. Acta* **705** 218–226.
- DE ROOI, J. J., RUCKEBUSCH, C. and EILERS, P. H. C. (2014). Sparse deconvolution in one and two dimensions: Applications in endocrinology and single-molecule fluorescence imaging. *Anal. Chem.* **86** 6291–6298.

- DENEUX, T., KASZAS, A., SZALAY, G., KATONA, G., LAKNER, T., GRINVALD, A., RÓZSA, B. and VANZETTA, I. (2016). Accurate spike estimation from noisy calcium signals for ultrafast three-dimensional imaging of large neuronal populations in vivo. *Nat. Commun.* **7** 12190.
- DOMBECK, D. A., KHABBAZ, A. N., COLLMAN, F., ADELMAN, T. L. and TANK, D. W. (2007). Imaging large-scale neural activity with cellular resolution in awake, mobile mice. *Neuron* **56** 43–57.
- FRIEDRICH, J. and PANINSKI, L. (2016). Fast active set methods for online spike inference from calcium imaging. In *Advances in Neural Information Processing Systems* 1984–1992.
- FRIEDRICH, J., ZHOU, P. and PANINSKI, L. (2017). Fast online deconvolution of calcium imaging data. *PLoS Comput. Biol.* **13** e1005423.
- FRYZLEWICZ, P. (2014). Wild binary segmentation for multiple change-point detection. *Ann. Statist.* **42** 2243–2281. [MR3269979](#)
- GENIE PROJECT (2015). Simultaneous imaging and loose-seal cell-attached electrical recordings from neurons expressing a variety of genetically encoded calcium indicators. [CRCNS.org](#).
- GREWE, B. F., LANGER, D., KASPER, H., KAMPA, B. M. and HELMCHEN, F. (2010). High-speed in vivo calcium imaging reveals neuronal network activity with near-millisecond precision. *Nat. Methods* **7** 399–405.
- HARCHAOU, Z. and LÉVY-LEDUC, C. (2010). Multiple change-point estimation with a total variation penalty. *J. Amer. Statist. Assoc.* **105** 1480–1493. [MR2796565](#)
- HASTIE, T., TIBSHIRANI, R. and FRIEDMAN, J. (2009). *The Elements of Statistical Learning: Data Mining, Inference, and Prediction*, 2nd ed. Springer, New York. [MR2722294](#)
- HASTIE, T., TIBSHIRANI, R. and WAINWRIGHT, M. (2015). *Statistical Learning with Sparsity: The Lasso and Generalizations. Monographs on Statistics and Applied Probability* **143**. CRC Press, Boca Raton, FL. [MR3616141](#)
- HAWRYLYCZ, M., ANASTASSIOU, C., ARKHIPOV, A., BERG, J., BUICE, M., CAIN, N., GOUWENS, N. W., GRATIY, S., IYER, R., LEE, J. H. et al. (2016). Inferring cortical function in the mouse visual system through large-scale systems neuroscience. *Proc. Natl. Acad. Sci. USA* **113** 7337–7344.
- HOCKING, T. D., RIGAILL, G., FEARNHEAD, P. and BOURQUE, G. (2017). A log-linear time algorithm for constrained changepoint detection. Preprint. Available at [ArXiv:1703.03352](#).
- HOLEKAMP, T. F., TURAGA, D. and HOLY, T. E. (2008). Fast three-dimensional fluorescence imaging of activity in neural populations by objective-coupled planar illumination microscopy. *Neuron* **57** 661–672.
- HUGELIER, S., DE ROOI, J. J., BERNEX, R., DUWÉ, S., DEVOS, O., SLIWA, M., DEDECKER, P., EILERS, P. H. and RUCKEBUSCH, C. (2016). Sparse deconvolution of high-density super-resolution images. *Sci. Rep.* **6**.
- JACKSON, B., SCARGLE, J. D., BARNES, D., ARABHI, S., ALT, A., GIOUMOUSIS, P., GWIN, E., SANGTRAKULCHAROEN, P., TAN, L. and TSAI, T. T. (2005). An algorithm for optimal partitioning of data on an interval. *IEEE Signal Process. Lett.* **12** 105–108.
- JOHNSON, N. A. (2013). A dynamic programming algorithm for the fused lasso and L_0 -segmentation. *J. Comput. Graph. Statist.* **22** 246–260. [MR3173713](#)
- KILLICK, R., FEARNHEAD, P. and ECKLEY, I. A. (2012). Optimal detection of changepoints with a linear computational cost. *J. Amer. Statist. Assoc.* **107** 1590–1598. [MR3036418](#)
- LEE, C.-B. (1995). Estimating the number of change points in a sequence of independent normal random variables. *Statist. Probab. Lett.* **25** 241–248. [MR1369518](#)
- LIN, K., SHARPNACK, J., RINALDO, A. and TIBSHIRANI, R. J. (2016). Approximate recovery in changepoint problems, from ℓ_2 estimation error rates. Preprint. Available at [ArXiv:1606.06746](#).
- MAIDSTONE, R., HOCKING, T., RIGAILL, G. and FEARNHEAD, P. (2017). On optimal multiple changepoint algorithms for large data. *Stat. Comput.* **27** 519–533. [MR3599687](#)
- MAMMEN, E. and VAN DE GEER, S. (1997). Locally adaptive regression splines. *Ann. Statist.* **25** 387–413. [MR1429931](#)

- MAZZONI, A., PANZERI, S., LOGOTHETIS, N. K. and BRUNEL, N. (2008). Encoding of naturalistic stimuli by local field potential spectra in networks of excitatory and inhibitory neurons. *PLoS Comput. Biol.* **4** e1000239, 20. [MR2476497](#)
- OLSHEN, A. B., VENKATRAMAN, E., LUCITO, R. and WIGLER, M. (2004). Circular binary segmentation for the analysis of array-based DNA copy number data. *Biostatistics* **5** 557–572.
- PNEVMATIKAKIS, E. A., MEREL, J., PAKMAN, A. and PANINSKI, L. (2013). Bayesian spike inference from calcium imaging data. In *Signals, Systems and Computers, 2013 Asilomar Conference on* 349–353. IEEE.
- PNEVMATIKAKIS, E. A., SOUDRY, D., GAO, Y., MACHADO, T. A., MEREL, J., PFAU, D., REARDON, T., MU, Y., LACEFIELD, C., YANG, W. et al. (2016). Simultaneous denoising, deconvolution, and demixing of calcium imaging data. *Neuron* **89** 285–299.
- PREVEDEL, R., YOON, Y.-G., HOFFMANN, M., PAK, N., WETZSTEIN, G., KATO, S., SCHRÖDEL, T., RASKAR, R., ZIMMER, M., BOYDEN, E. S. et al. (2014). Simultaneous whole-animal 3D imaging of neuronal activity using light-field microscopy. *Nat. Methods* **11** 727–730.
- QIAN, J. and JIA, J. (2012). On pattern recovery of the fused lasso. Preprint. Available at [ArXiv:1211.5194](#).
- RINALDO, A. (2009). Properties and refinements of the fused lasso. *Ann. Statist.* **37** 2922–2952. [MR2541451](#)
- ROJAS, C. R. and WAHLBERG, B. (2014). On change point detection using the fused lasso method. Preprint. Available at [ArXiv:1401.5408](#).
- SASAKI, T., TAKAHASHI, N., MATSUKI, N. and IKEGAYA, Y. (2008). Fast and accurate detection of action potentials from somatic calcium fluctuations. *J. Neurophysiol.* **100** 1668–1676.
- SCOTT, A. J. and KNOTT, M. (1974). A cluster analysis method for grouping means in the analysis of variance. *Biometrics* **30** 507–512.
- THEIS, L., BERENS, P., FROUDARAKIS, E., REIMER, J., ROSÓN, M. R., BADEN, T., EULER, T., TOLIAS, A. S. and BETHGE, M. (2016). Benchmarking spike rate inference in population calcium imaging. *Neuron* **90** 471–482.
- TIBSHIRANI, R., SAUNDERS, M., ROSSET, S., ZHU, J. and KNIGHT, K. (2005). Sparsity and smoothness via the fused lasso. *J. R. Stat. Soc. Ser. B. Stat. Methodol.* **67** 91–108. [MR2136641](#)
- VAN ROSSUM, M. C. (2001). A novel spike distance. *Neural Comput.* **13** 751–763.
- VICTOR, J. D. and PURPURA, K. P. (1996). Nature and precision of temporal coding in visual cortex: A metric-space analysis. *J. Neurophysiol.* **76** 1310–1326.
- VICTOR, J. D. and PURPURA, K. P. (1997). Metric-space analysis of spike trains: Theory, algorithms and application. *Network* **8** 127–164.
- VOGELSTEIN, J. T., WATSON, B. O., PACKER, A. M., YUSTE, R., JEDYNAK, B. and PANINSKI, L. (2009). Spike inference from calcium imaging using sequential Monte Carlo methods. *Biophys. J.* **97** 636–655.
- VOGELSTEIN, J. T., PACKER, A. M., MACHADO, T. A., SIPPY, T., BABADI, B., YUSTE, R. and PANINSKI, L. (2010). Fast nonnegative deconvolution for spike train inference from population calcium imaging. *J. Neurophysiol.* **104** 3691–3704.
- VOLGUSHEV, M., ILIN, V. and STEVENSON, I. H. (2015). Identifying and tracking simulated synaptic inputs from neuronal firing: Insights from in vitro experiments. *PLoS Comput. Biol.* **11** e1004167.
- YAKSI, E. and FRIEDRICH, R. W. (2006). Reconstruction of firing rate changes across neuronal populations by temporally deconvolved Ca²⁺ imaging. *Nat. Methods* **3** 377–383.
- YAO, Y.-C. (1988). Estimating the number of change-points via Schwarz' criterion. *Statist. Probab. Lett.* **6** 181–189. [MR0919373](#)
- YAO, Y.-C. and AU, S. T. (1989). Least-squares estimation of a step function. *Sankhyā Ser. A* **51** 370–381. [MR1175613](#)

ZOU, H. (2006). The adaptive lasso and its oracle properties. *J. Amer. Statist. Assoc.* **101** 1418–1429.
MR2279469

DEPARTMENT OF STATISTICS
UNIVERSITY OF WASHINGTON
SEATTLE, WASHINGTON 98195
USA
E-MAIL: swjewell@uw.edu

DEPARTMENTS OF STATISTICS AND BIostatISTICS
UNIVERSITY OF WASHINGTON
SEATTLE, WASHINGTON 98195
USA
E-MAIL: dwitten@uw.edu